Turbulence coherence and its impact on wind-farm power fluctuations

Nicolas Tobin[1] **and Leonardo P. Chamorro**[1,2,3,†]

[1]Department of Mechanical Engineering, University of Illinois, Urbana, IL 61801, USA

[2]Department of Civil and Environmental Engineering, University of Illinois, Urbana, IL 61801, USA

[3]Department of Aerospace Engineering, University of Illinois, Urbana, IL 61801, USA

Using a physics-based approach, we infer the impact of the coherence of atmospheric turbulence on the power fluctuations of wind farms. Application of the random-sweeping hypothesis reveals correlations characterized by advection and turbulent diffusion of coherent motions. Those contribute to local peaks and troughs in the power spectrum of the combined units at frequencies corresponding to the advection time between turbines, which diminish in magnitude at high frequencies. Experimental inspection supports the results from the random-sweeping hypothesis in predicting spectral characteristics, although the magnitude of the coherence spectrum appears to be over-predicted. This deviation is attributed to the presence of turbine wakes, and appears to be a function of the turbulence approaching the first turbine in a pair.

Key words: turbulent boundary layers, turbulent flows

---

1. Introduction

Wind-power variability occurs across a range of spatial and temporal scales due to several physical processes. Over very large scales, the summed power output of several geographically distant wind farms is smoothed due to individual wind farms being relatively uncorrelated. Whereas the power spectral density of the power output of a single turbine, or a small wind farm, has been shown to follow a power law of $\omega^{-5/3}$ (Apt 2007), where ω is angular frequency, Katzenstein, Fertig & Apt (2010) observed a behaviour of $\omega^{-2.56}$ when considering the aggregated power of 20 wind farms. Bandi (2017) later deduced a limit to the smoothing that can be achieved with wide geographic separation, corresponding to a power-law behaviour of $\omega^{-7/3}$, arguing that the power fluctuations from many aggregate wind farms are dominated by the immutable variability of individual wind farms.

The $\omega^{-5/3}$ power law observed by Apt (2007) has been explained as stemming from the Kolmogorov $-5/3$ law for isotropic turbulence (Kolmogorov 1941), as the power spectrum of a turbulent signal raised to any power will exhibit the same $\omega^{-5/3}$ behaviour (Milan, Wächter & Peinke 2013; Tabar *et al.* 2014; Bandi 2017; Bossuyt, Meneveau & Meyers 2017). This is relevant to the power spectra of wind turbines

† Email address for correspondence: lpchamo@illinois.edu

since $P \propto u^3$, where P is power and u is the wind speed. However, deviations from $\omega^{-5/3}$ scaling have been observed at time scales typically smaller than tens of seconds for both wind farms and individual turbines, corresponding to the response time of a wind turbine (Apt 2007; Milan *et al.* 2013; Chamorro *et al.* 2015; Bandi 2017). Tobin, Zhu & Chamorro (2015) sought to analytically explain deviation from Kolmogorov scaling due to rotor inertia, and arrived at a $\omega^{-11/3}$ power law. A trend consistent with this is seen in the spectra of Anvari *et al.* (2016). However, other processes have been shown to play a role in short-term power fluctuations. For instance, Anvari, Wächter & Peinke (2017) observed high-frequency wind-farm fluctuations being affected on short time scales by the phase locking of the fluctuations of pairs of turbines.

Further, it has been observed (Stevens & Meneveau 2014) that the spectra of aggregate wind-farm power exhibit characteristic peaks at integer multiples of the advective frequency $\omega_a = 2\pi/t_a$, where t_a is the time it takes for a passive tracer particle to travel between turbines. In attempting to explain this behaviour, formulations by Liu *et al.* (2017) and Bossuyt *et al.* (2017) linked the power-production spectrum to the velocity spectrum, and incorporated the Kraichnan–Tennekes random-sweeping hypothesis (RSH) (Kraichnan 1964; Tennekes 1975) to match with experimental wind-tunnel data. However, their approaches differed slightly; Bossuyt *et al.* treated the problem as a discrete sampling of the boundary layer, whereas Liu *et al.* focused on formulations for the two-point cross-spectrum. The RSH assumes that the turbulent velocity field is randomly advected by a large-scale sweeping velocity, and has been shown to be useful in modelling spatio-temporal spectra in turbulent boundary layers (Wilczek, Stevens & Meneveau 2015).

We attempt to explain the advection phenomenon by expanding on the work from Liu *et al.* (2017) to derive analytical expressions for the cross-spectrum, and related coherence, of the power output of wind-turbine pairs using the RSH. We further test the ability of the RSH to predict the spectral correlation characteristics between turbine pairs with experimental wind-tunnel data across a range of flow characteristics, and evaluate the simplifying assumption used in both works that turbines act as passive probes of the turbulence.

2. Cross-spectra of wind-turbine pairs

2.1. *Coherence spectrum*

Consider the power spectrum $\Phi(\omega)$ of a signal $X(t)$, which is defined as the Fourier transform of the signal's autocovariance function $\gamma(\tau) = \langle X(t)X(t+\tau) \rangle$, as follows

$$\Phi_X(\omega) = \int_{-\infty}^{\infty} \langle X(t)X(t+\tau) \rangle \mathrm{e}^{-\mathrm{i}\omega\tau} \, \mathrm{d}\tau. \tag{2.1}$$

Here, $\langle \cdot \rangle$ denotes the expected value. For a combined signal $X(t) = X_1(T) + X_2(t)$, the autocovariance includes covariance terms, namely $\gamma_{1,2}$ and $\gamma_{2,1}$, i.e.

$$\gamma_X = \langle [X_1(t) + X_2(t)][X_1(t+\tau) + X_2(t+\tau)] \rangle = \gamma_1 + \gamma_2 + \gamma_{1,2} + \gamma_{2,1}, \tag{2.2}$$

where $\gamma_{1,2}(\tau) = \gamma_{2,1}(-\tau)$. This can be generalized to any number of combined signals X_i for $i = 1, 2, \ldots, N$ as:

$$\gamma_N = \sum_{i=1}^{N} \gamma_i + \sum_{i=1}^{N-1} \sum_{j=i+1}^{N} [\gamma_{i,j} + \gamma_{j,i}]. \tag{2.3}$$

Because $\gamma_{1,2}$ and $\gamma_{2,1}$ are mirrored about $\tau = 0$, their Fourier transforms are complex conjugates. Therefore, the combined power spectrum of the N signals is given by:

$$\Phi_N = \sum_{i=1}^{N} \Phi_i + 2 \sum_{i=1}^{N-1} \sum_{j=i+1}^{N} \text{Re}(\Phi_{i,j}), \qquad (2.4)$$

where $\Phi_{i,j}$ is the cross-spectrum of the signals X_i and X_j, and $\text{Re}(\cdot)$ is the real-part operator. When the two signals are perfectly correlated, $|\Phi_{i,j}| = (\Phi_i \Phi_j)^{1/2}$. It is therefore natural to define the coherence spectrum $C_{i,j}$ as

$$C_{i,j}(\omega) = \frac{\Phi_{i,j}(\omega)}{\sqrt{\Phi_i(\omega)\Phi_j(\omega)}}, \qquad (2.5)$$

although other related definitions exist.

2.2. *The random-sweeping hypothesis*

To predict the coherence of wind-turbine pairs, we use the Kraichnan–Tennekes random-sweeping hypothesis (Kraichnan 1964; Tennekes 1975). In order to apply the RSH to turbine power production, it is convenient to treat wind turbines as passive probes of the turbulence so that the flow is laterally homogeneous. This is clearly not true, as turbine wakes are an important flow characteristic in wind farms. This assumption will be evaluated by the data. The RSH assumes that the turbulent velocity $\boldsymbol{u}'$ does not evolve temporally, but is advected by a large-scale sweeping velocity $\boldsymbol{v}$, i.e.

$$\frac{\partial \boldsymbol{u}'}{\partial t} + \boldsymbol{v} \cdot \frac{\partial \boldsymbol{u}'}{\partial \boldsymbol{x}} = 0. \qquad (2.6)$$

The assumption that the small-scale turbulent field and the large-scale sweeping velocity do not nonlinearly interact cannot be strictly true, though it is attractive for its ability to make analytical expressions for turbulence spectra. Moreover, the RSH has been shown to make good predictions for spatio-temporal spectra in turbulent boundary layers (Wilczek *et al.* 2015). The terms $\boldsymbol{u}'$ and $\boldsymbol{v}$ in (2.6) are both vectorial. However, if the coordinate axes are defined such that u_1 is aligned with the mean wind and the yaw of the wind turbines, the other components can be ignored in estimating power fluctuations. Furthermore, since $\langle u_1'^2 \rangle$ is typically much larger than $\langle u_2'^2 \rangle$ and $\langle u_3'^2 \rangle$ in a turbulent boundary layer, equation (2.6) reduces to:

$$\frac{\partial u_1'}{\partial t} + (V_1 + v_1')\frac{\partial u_1'}{\partial x_1} = 0, \qquad (2.7)$$

where u_1' is the turbulent streamwise velocity fluctuation, V_1 is the mean sweeping velocity, taken as the hub-height velocity of the approaching boundary layer, and v_1' is the fluctuating streamwise sweeping velocity.

The Fourier transform (denoted with the symbol $\widehat{o}$) of (2.7) with respect to t conveniently converts the expression to an ordinary differential equation in x_1 for $\hat{u}(x_1, \omega)$, as follows:

$$\frac{\partial \hat{u}(x_1, \omega)}{\partial x} = -\frac{\mathrm{i}\omega}{V + v'}\hat{u}(x_1, \omega). \qquad (2.8)$$

If v' and u' are statistically independent, the cross-spectrum of the turbulent fluctuations at two points separated by a distance Δx in the streamwise direction can then be expressed as:

$$\Phi_{0,\Delta x} = \langle \hat{u}(\Delta x, \omega)\hat{u}(0, -\omega) \rangle = \langle \hat{u}(0, \omega)\hat{u}(0, -\omega) \rangle \left\langle \exp\left(\frac{-i\omega\Delta x}{V + v'}\right) \right\rangle. \quad (2.9)$$

Here, we have assumed that the spectra at points 0 and Δx are statistically identical. If v'_1 is further assumed small compared to V_1, and to have a Gaussian probability distribution with zero mean and variance σ_v^2, equation (2.9) can be integrated over the probability distribution of v':

$$\Phi_{0,\Delta x} \simeq \frac{\langle \hat{u}(0, \omega)\hat{u}(0, -\omega) \rangle}{\sqrt{2\pi\sigma_v^2}} \int_{-\infty}^{\infty} \exp\left(\frac{-i\omega\Delta x}{V} + \frac{i\omega\Delta x v'}{V^2}\right) \exp\left(-\frac{v'^2}{2\sigma_v^2}\right) \mathrm{d}v'. \quad (2.10)$$

The evaluation of the integral in (2.10) leads to:

$$\Phi_{0,\Delta x} = \langle \hat{u}(0, \omega)\hat{u}(0, -\omega) \rangle \times \exp\left(-\frac{i\omega\Delta x}{V}\right) \exp\left(-\frac{\omega^2\Delta x^2\sigma_v^2}{2V^4}\right). \quad (2.11)$$

Making the further assumption that the lateral behaviour of the covariance function $\langle u'(x, y, t)u'(0, 0, 0) \rangle$ is separable, and takes the form of an exponential decay with a length parameter L_y (Lukassen *et al.* 2018), the final expression for the cross-spectrum is:

$$\Phi_{0,\Delta x} = \Phi(0, 0, \omega) \times \exp\left(-\frac{i\omega\Delta x}{V}\right) \exp\left(-\frac{\omega^2\Delta x^2\sigma_v^2}{2V^4}\right) \exp\left(\frac{\Delta y^2}{L_y^2}\right). \quad (2.12)$$

So far, we have shown only the correlation behaviour between two points $(0, 0)$ and $(\Delta x, \Delta y)$ that have statistically identical spectra, with all the turbulence kinetic energy at the downwind point having simply advected downwind. However, this does not describe the two points immediately upwind of two wind turbines, since the wake from the upwind unit adds turbulence scales to the downwind counterpart and, therefore, statistically different turbulent characteristics. Nevertheless, we proceed with this assumption as a limiting estimate in the case where wake motions are dominated by atmospheric boundary layer (ABL) motions, and test this estimate when far from the limiting behaviour. Then, a closed-form expression for the coherence can be taken as

$$C_{i,j}(\omega) = \exp\left(-\frac{i\omega\Delta x}{V}\right) \times \exp\left(-\frac{\omega^2\Delta x^2\sigma_v^2}{2V^4}\right) \exp\left(\frac{\Delta y^2}{L_y^2}\right). \quad (2.13)$$

The interpretation of this result is that large-scale atmospheric motions impart their signature on an upwind turbine, are distorted as they are advected downstream, and impart a similar signature on a downwind turbine, with higher frequency scales being the more distorted. This high-frequency distortion is consistent with the findings of Vigueras-Rodríguez *et al.* (2010), who observed velocity correlations to be the highest for low frequencies within a wind farm. This is conceptually shown in figure 1. The proposed model is similar in construction to existing empirical formulations used
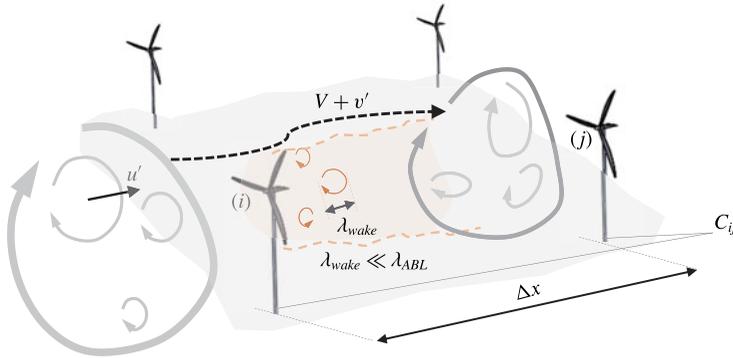
FIGURE 1. (Colour online) Conceptual schematic illustrating the factors impacting turbine–turbine coherence. Atmospheric motions of length scale λ_{ABL} are advected and partially distorted by large-scale sweeping. Wake motions of length scale $\lambda_{wake} \ll \lambda_{ABL}$ are introduced by turbines, and do not contribute to coherence.

throughout the literature broadly stemming from the Panofsky & Dutton (1984) model of longitudinal velocity coherence,

$$C_{PD} = \exp\left(-\frac{As\omega}{V}\right), \qquad (2.14)$$

where s is the separation between two points and A is an empirical constant, which changes depending on whether the separation is lateral or longitudinal, as well as the local turbulence characteristics. Interestingly, Panofsky & Dutton (1984) suggested $A \approx \sigma_v/V$ for streamwise separations based only on heuristic arguments, showing a close relation to the present formulation. However, that coherence spectrum differs from that proposed here, with $\Phi_{i,j}$ in (2.5) being replaced by $|\Phi_{i,j}|$, eliminating phase information. To avoid confusion, we refer to this alternative definition as the absolute coherence. The Panofsky–Dutton model is based on an observation by Davenport (1961) that the absolute coherence is well approximated by a simple exponential decay with a fitted decay rate; it was used by Jimenez *et al.* (2008) to model the absolute coherence of two points with small separation in a boundary layer, both with and without turbine wakes. They found the coherence from both a set of experiments and large-eddy simulations to be well estimated, though these results were only for the velocity components, and not power from turbine pairs. Sørensen *et al.* (2008), however, modelled the power coherence between turbine pairs in the Nysted and Horns Rev wind farms in Denmark, using the modified Panofsky–Dutton coherence model of Schlez & Infield (1998), and showed good agreement with their experimental data.

3. Experiments

A set of experiments was performed with model wind-turbine arrays operated in the wind tunnel of the Renewable Energy and Turbulent Environment Group (RE-TE-G) at the University of Illinois to test the coherence predictions of the RSH. The wind tunnel has a test section 6 m long, 0.46 m high and 0.9 m wide. Details of the facility can be found in Adrian, Meinhart & Tomkins (2000). To assess the impact

of both turbulence intensity $I_u = \sigma_u/U_0$ (where σ_u and U_0 are the standard deviation and mean of the incoming velocity at hub height), and integral time scales $T_u = \int_0^\infty \langle u'(t)u'(t+\tau) \rangle \, d\tau$, power fluctuations of wind turbines within various wind-farm layouts were acquired for a range of turbulence characteristics.

Four flow regimes were examined; two consisted of uniform incoming flows with very low ($I_u = 0.3\%$) and high ($I_u = 3.0\%$) turbulence levels. The other two cases consisted of turbulent boundary layers. One was developed over a nearly smooth wall with a roughness height z_0 of 0.019 mm, and $I_u = 8.0\%$ at hub height; the other developed over a rough wall with $z_0 = 0.52$ mm, and $I_u = 10\%$ at hub height. For all cases, except the laminar free-stream flow, an active turbulence generator was placed at the inlet to lead to the formation of large-scale turbulent motions; see Tobin, Hamed & Chamorro (2017) for details.

The model turbines had a rotor diameter $d_T = 0.12$ m, and were based on a model hydrokinetic turbine from Sandia National Labs (Shiu *et al.* 2012; Johnson *et al.* 2013). The rotors were attached to a Precision Microdrives 112-001 Micro Core 12 mm motor which acted as the loading system and a method to measure the power output, where rated power resulted $P_0 \approx 1$ W. The tip-speed ratio λ was kept constant at $\lambda = 5.0$ by adjusting the resistance across the generator. The power output was sampled at a rate of 100 kHz for a duration of 480 s. Power was calculated from the applied resistance, and the voltage across the terminals of the generators as measured with a data acquisition system individually for each turbine. The turbines were identical to those used in Tobin *et al.* (2017), and have power and thrust coefficients of 0.45 and 0.79, respectively. The power coefficient was inferred from the mean measured power, making adjustments based on the efficiency curve of the generator. The thrust coefficient is based on wake deficit measurements.

The experiments were conducted with an incoming hub-height velocity of $U_0 = 9.0$ m s^{-1}, which varied by $\pm 5\%$ between flow cases; this resulted in a Reynolds number $Re = U_0 d_T/\nu \approx 7.2 \times 10^4$. Flow was also measured in the upwind vicinity of each turbine that had power measurements taken to characterize the local incoming flow. Velocity measurements were done via hot-wire, and were sampled at a rate of 10 kHz for a duration of 60 s. For all flow cases, three streamwise columns of turbines were used, spaced $S_y = 2.5$ rotor diameters apart, and the power was sampled only from the central column. The uniform flow cases used three rows of turbines, with streamwise spacings of $S_x = 5$, 7 and 10 rotor diameters. The boundary-layer cases used four rows of turbines, with streamwise spacings of $S_x = 7$ and 10 rotor diameters and hub height $z_h = 0.125$ m. Conceptual schematics are shown for the uniform flow in figure 2(*a*), and for the boundary-layer flow in figure 2(*b*). In all experiments, the last row was laterally displaced from the preceding rows, with a displacement of 0, 0.5, or 1.0 rotor diameters to investigate the effect of lateral displacement.

4. Evaluation of the model

Each set of data was split into ten equally sized non-overlapping windows. The estimated coherence $\tilde{C}$ of each turbine pair was found by averaging the coherence of each subset of data. This was used to verify the fidelity of the RSH predictions on the two characteristic frequencies related to advection (ω_a) and turbulent decoherence (ω_c). However, the prediction from the RSH that coherence reaches unity at zero frequency was not supported by the data, and the magnitude of the coherence was
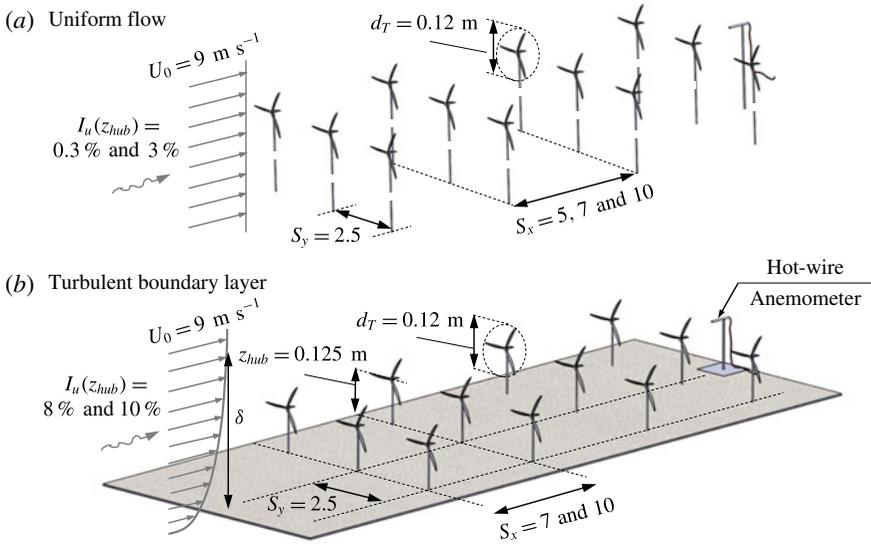
N. Tobin and L. P. Chamorro

FIGURE 2. Basic schematics of the experimental set-ups; wind farms in (*a*) uniform flow, and (*b*) turbulent boundary layer.

lower than predicted. We model this reduced magnitude with a multiplicative constant *a*, and calculate *a* for each turbine pair via least-squares fit as:

$$a = \underset{a}{\operatorname{argmin}} \sum_{j=1}^{n} \left| \tilde{C}_j - a \exp\left(\frac{-i\omega_j \Delta x}{U_0} \right) \exp\left(-\frac{\omega_j^2 \Delta x^2 \sigma_u^2}{2U_0^4} \right) \right|^2, \quad (4.1)$$

where *n* is the number of frequencies at which the coherence is calculated. Some coherence measurements were unreliable, as not enough data were taken to estimate a clear spectrum. This was particularly common for turbine pairs separated by more than 2 rows, or when the flow approaching the first turbine in a pair had low turbulence. As such, data are reported only when the modelled power spectrum fits the data with $R^2 > 0.2$.

The advection frequency was measured from the data based on the angle of the coherence spectrum $\theta = \angle \tilde{C}$. The RSH predicts that this quantity changes with frequency as follows:

$$\frac{d\theta}{d\omega} = -\frac{\Delta x}{U_0} = -\frac{2\pi}{\omega_a}. \quad (4.2)$$

Then, for each turbine–turbine pair, θ was modelled as:

$$\theta = -\left(\frac{2\pi\omega}{\omega_a} \mod 2\pi \right) + \pi; \quad (4.3)$$

the ω_a values which minimize the squared error with the experimental values of $\angle \tilde{C}$ are reported as $\tilde{\omega}_a$, where $\tilde{\circ}$ denotes a value fitted from the data. Examples of the modelled and measured coherence angle are shown in figure 3. Finally, the measured decoherence frequency $\tilde{\omega}_c$ is reported as the result of a final least-squares fit of the coherence spectrum.
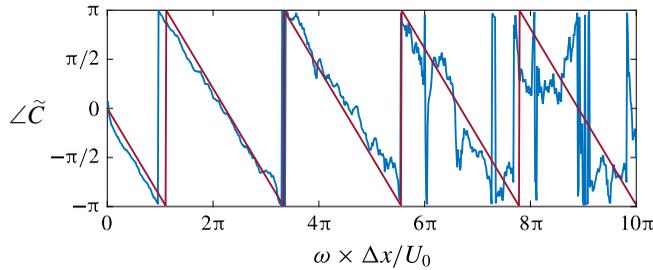
FIGURE 3. (Colour online) Modelled and measured coherence phase angle $\angle \tilde{C}$.

Two phenomena may contribute to the parameter a in (4.1). The first is lateral displacement, in which case $a = \exp(\Delta y^2/L_y^2)$. However, there may also be a contribution from the perturbed incoming flow by the turbine wake, such that $a \neq 1$ when $\Delta y = 0$. Because turbines act approximately as probes of the turbulence, power coherence can be taken as roughly equal to the coherence of two points immediately upwind of each turbine in the pair. Without either turbine present, the coherence of these two points should be closely approximated by the RSH (Wilczek *et al.* 2015). However, the correlation between these two points is affected by wake motions induced by the upwind turbine in the pair, which we model with the multiplicative constant a.

The least-squares estimates of the characteristic frequencies ω_a and ω_c are compared to their theoretical counterparts as predicted earlier. Namely, we should expect that

$$\omega_a = \frac{2\pi U_0}{\Delta x}, \qquad (4.4)$$

and

$$\omega_c = \frac{U_0^2}{\Delta x \sigma_v}. \qquad (4.5)$$

The particular exponential behaviour of the power spectrum is quite consistent with the data; an example is illustrated in figure 4. The least-squares estimates for ω_a and ω_c closely fit the predictions, with $R^2 = 0.85$ and 0.87, respectively, suggesting a strong predictive ability for these two quantities. Measured values of the two characteristic frequencies are compared with their predictions in figures 5 and 6.

The data suggest that the zero-frequency coherence magnitude a is dependent primarily on the turbulence intensity I_u of the flow approaching the most upwind turbine in a pair. A wide range of I_u is achieved by considering the flow approaching each individual upwind turbine, which may be impacted by the presence of upwind wakes. This is evident with a linear regression between a and I_u, such that $a = \alpha_0 + \alpha_1 I_u$. The characteristic constant α_1 is found to have a 95 % confidence bound between 1.29 and 2.47, clearly suggesting that higher approaching I_u leads to higher coherence. A similar regression test between a and the integral time scale T_u shows that no statistically significant trend exists between them. This is an interesting result, since an assumption of the RSH is a wide separation of scales between the sweeping velocity and the process of interest. It would therefore be useful to assess the impact of atmospheric stability on power coherence, since lower I_u is generally associated with the clear-night stable boundary layer; furthermore, interaction between turbine wakes and the boundary layer is modulated by atmospheric stability. For instance,
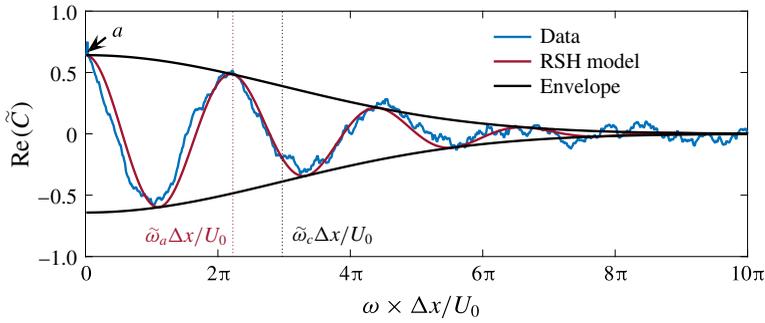
FIGURE 4. (Colour online) Sample coherence data from the rough-wall boundary layer experiment considering a wind farm with $S_x = 10$.
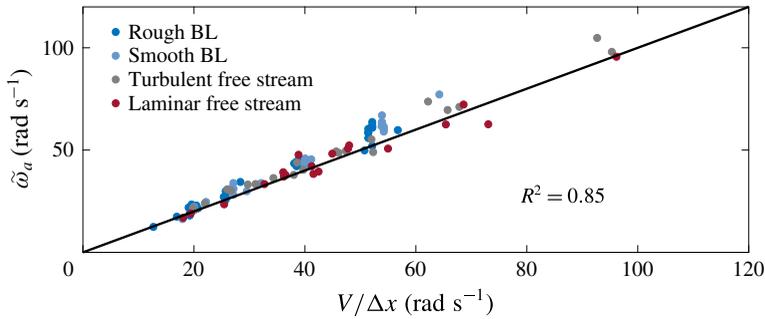

FIGURE 5. (Colour online) Comparison of the measured and theoretical characteristic advection frequency (ω_a) for various flow conditions.
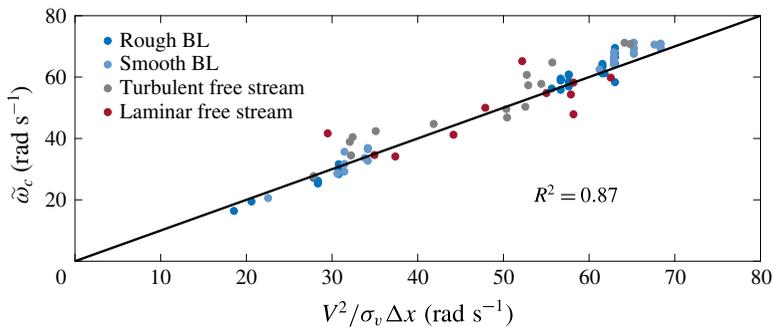

FIGURE 6. (Colour online) Comparison of the measured and theoretical characteristic frequency of the turbulence decoherence (ω_c) for various flow conditions.

Abkar & Porté-Agel (2015) found major differences in wake growth characteristics between different atmospheric stability states, and both Lu & Porté-Agel (2011) and Cortina, Calaf & Cal (2016) found significant impacts on vertical and horizontal mixing of momentum for different stability regimes.

We argue that the deviation of the turbulence coherence trend from the RSH is a result of the induced motions from turbine wakes, which are significantly weakly correlated with the incoming turbulence (Espana *et al.* 2012). Since wake-added motions are comparatively small (Chamorro *et al.* 2012; Tian, Ozbay & Hu 2018), they may evolve sufficiently between rows of turbines to contribute to power fluctuations in the downwind turbine that are not correlated with the upwind counterpart. This is consistent with the findings of Tian, Ozbay & Hu (2014), who noted faster dissipation and earlier breakdown of the wake vortices under high turbulence inflow, as well as the findings of Lignarolo *et al.* (2015), who argue that wake motions are dominated by tip-vortex breakdown. We proceed to test this hypothesis, at least in its limiting behaviour, as follows.

Consider wake-added velocity fluctuations u'_w added to the upwind velocity fluctuations u'_u, which determines the total velocity fluctuations approaching the downwind turbine in a pair u'_{tot}, as follows:

$$u'_{tot} = L_{\delta t} u'_u + u'_w, \tag{4.6}$$

where $L_{\delta t}$ is the lag operator with lag time δt, so that upwind velocity fluctuations are advected without evolving. With the previous assumption that the coherence of the turbine power is the same as the coherence of the velocity fluctuations immediately upwind of each turbine, the absolute coherence takes the form

$$|C| = \frac{|\widehat{u}_u \widehat{(L_{\delta t} u_u + \widehat{u}_w)^*}|}{(\widehat{u}_u \widehat{u}_u^* \widehat{u}_{tot} \widehat{u}_{tot}^*)^{1/2}}, \tag{4.7}$$

where ( )* denotes the complex conjugate. In the limiting case where u'_w is uncorrelated with u'_u, the numerator of (4.7) is the power spectrum of the upwind point. This estimate for $|C|$ is then an upper bound in the case where wake motions are uncorrelated with the turbine from which they are shed, and reduces to $|C| = \sqrt{\Phi_u/\Phi_{tot}}$. A coherence estimate greater than this upper bound would lead us to reject the hypothesis that a turbine's power output is uncorrelated with its wake-added turbulence. No turbine–turbine pair was found to have a coherence value higher than this bound with statistical significance for frequencies below $2\pi U/d_T$. A more thorough investigation of this hypothesis should include simultaneous measurements of power as well as upstream and downstream velocity fluctuations.

In general, smaller values of a are found for turbine pairs spanning more than two rows. Representative examples of coherence spectra for turbines separated by one, two, and three rows for the case with $S_x = 7$ and $S_y = 0$ in the nearly smooth-wall boundary layer are shown in figure 7; there, coherence clearly decreased with increased number of rows separating the turbines in a pair. The general trend towards lower a with greater numbers of rows separating the turbines is evident in all four flow cases, as illustrated in figure 8(*a*). This figure shows the average a measured for all turbine–turbine pairs in a given flow case with a given number of rows separating them and, therefore, shows bulk behaviour. This trend is consistent with the interpretation that wake-added motions detract from turbine–turbine coherence, since a greater fraction of the turbulence impacting turbines deep within a wind farm is from wake-added motions. Figure 8(*a*) additionally suggests a clear trend toward higher coherence values with greater ambient turbulence intensity.

Larger inter-turbine spacing also led to lower coherence, with a trend towards lower a with greater spacing, as shown in figure 8(*b*). The interpretation of this
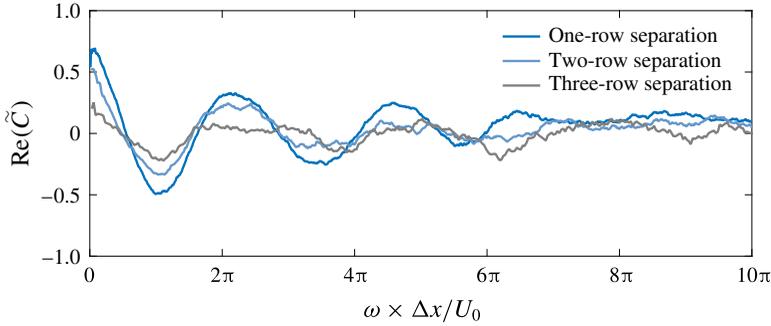
FIGURE 7. (Colour online) Example of coherence spectra in the case of the smooth-wall boundary layer, with streamwise separation $S_x = 7$ and $S_y = 0$.
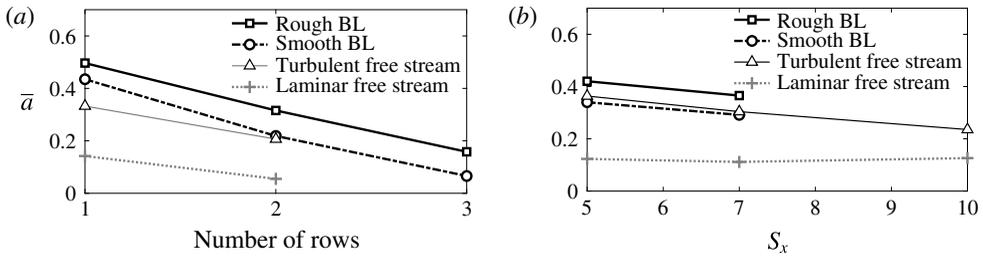

FIGURE 8. Trends of average coherence magnitude for each flow case with (*a*) number of rows separating turbines, and (*b*) inter-turbine spacing.

result in the argument that wake-added motions detract from coherence is unclear. If atmospheric motions are expected to dominate turbine–turbine correlations, it might be expected that coherence would increase with greater inter-turbine spacing as wakes would be given more distance to dissipate. Conversely, greater inter-turbine spacing would provide more time for wake motions to nonlinearly interact with and distort atmospheric motions.

The effect of lateral displacement is not conclusive from the data; no significant trend is found to occur in the cases considered. However, this may be expected, since lateral separation leads to two competing results. The first is that correlation is simply reduced as a result of greater separation distance, and a reduction similar to the separable behaviour posited in (2.13) is expected. In addition, lateral separation implies that the downwind turbine in a pair is exposed to fewer uncorrelated wake motions, and coherence might be expected to increase. A clearer trend might therefore be observed when considering lateral separations larger than one rotor diameter.

The data also allow testing the modelling assumption that v'_1 is comparatively small and Gaussian. The model coherence from (2.9) is evaluated by averaging $\exp(-i\omega\Delta x/(V + v'))$ for a range of frequencies using the time-series velocity data from the last row of the $S_x = 7$ wind farm in the rough-wall scenario, as shown in figure 9. This particular velocity time series was chosen because it had the largest turbulence intensity, $I_u = 13.3\%$, which stresses the assumption of small v' the greatest. The application of the Kolmogorov–Smirnov test indicates that the velocity approaching this turbine is non-Gaussian. Nonetheless, the difference between the empirical coherence model and the Gaussian model is minor, even in the limiting case.
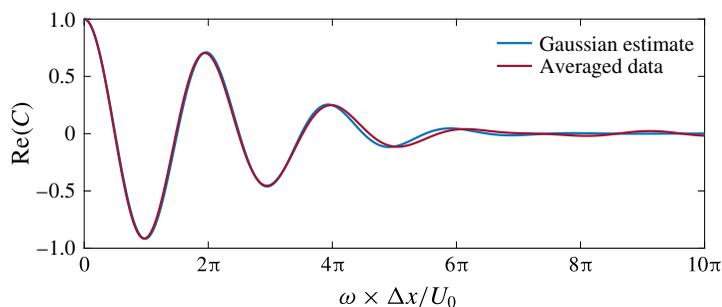
FIGURE 9. (Colour online) Model coherence spectrum given velocity time series approaching the last row of turbines in the case of rough-wall boundary layer, with streamwise separation $S_x = 7$. The difference between the Gaussian estimate and the empirical model is negligible.

5. Conclusion

The RSH does well in predicting the general behaviour of the coherence of wind-turbine pairs. The complex exponential structure predicted is observed in the experimental data, with strong agreement with the characteristic frequency scales predicted by the RSH. However, the turbine wakes appear to diminish the magnitude of the coherence by a multiplicative constant $a \in (0, 1)$, which depends strongly on the structure of the flow approaching the first turbine in a pair. Namely, for flows with high-energy, large motions have the largest values of a. The data suggest that this may be explained by the assumption that turbine-added wake motions are uncorrelated with the turbine from which they are shed. Though similarities exist between the Panofsky–Dutton model and the current model, the final expressions differ, as well as the method employed in arriving to them, with the current model being less empirical. Furthermore, the current experimental results suggest that the magnitude of the coherence predicted either with the Panofsky–Dutton model or the RSH is too high, so that aggregate wind-farm power fluctuations may be improperly estimated without modification to the coherence models to account for wake-added motions, either of the type proposed or similar.

It is still not clear how the turbulence induced in the turbine wake impacts the coherence. A physical framework which accounts for the described observations is therefore desirable. It should also be noted that similar results in arrays of vertical-axis wind turbines may prove distinctly different, due to the differing momentum flux and wake growth characteristics in these types of wind farms (Kinzel, Araya & Dabiri 2015; Abkar & Dabiri 2017).

Acknowledgements

REFERENCES

ABKAR, M. & DABIRI, J. O. 2017 Self-similarity and flow characteristics of vertical-axis wind turbine wakes: an les study. *J. Turbul.* **18** (4), 373–389.

ABKAR, M. & PORTÉ-AGEL, F. 2015 Influence of atmospheric stability on wind-turbine wakes: a large-eddy simulation study. *Phys. Fluids* **27** (3), 035104.

ADRIAN, R. J., MEINHART, C. D. & TOMKINS, C. D. 2000 Vortex organization in the outer region of the turbulent boundary layer. *J. Fluid Mech.* **422**, 1–54.

ANVARI, M., LOHMANN, G., WÄCHTER, M., MILAN, P., LORENZ, E., HEINEMANN, D., TABAR, M. R. R. & PEINKE, J. 2016 Short term fluctuations of wind and solar power systems. *New J. Phys.* **18** (6), 063027.

ANVARI, M., WÄCHTER, M. & PEINKE, J. 2017 Phase locking of wind turbines leads to intermittent power production. *Europhys. Lett.* **116** (6), 60009.

APT, J. 2007 The spectrum of power from wind turbines. *J. Power Sources* **169** (2), 369–374.

BANDI, M. M. 2017 Spectrum of wind power fluctuations. *Phys. Rev. Lett.* **118** (2), 028301.

BOSSUYT, J., MENEVEAU, C. & MEYERS, J. 2017 Wind farm power fluctuations and spatial sampling of turbulent boundary layers. *J. Fluid Mech.* **823**, 329–344.

CHAMORRO, L. P., GUALA, M., ARNDT, R. E. A. & SOTIROPOULOS, F. 2012 On the evolution of turbulent scales in the wake of a wind turbine model. *J. Turbul.* **13**, N27.

CHAMORRO, L. P., LEE, S.-J., OLSEN, D., MILLIREN, C., MARR, J., ARNDT, R. E. A. & SOTIROPOULOS, F. 2015 Turbulence effects on a full-scale 2.5 mw horizontal-axis wind turbine under neutrally stratified conditions. *Wind Energy* **18** (2), 339–349.

CORTINA, G., CALAF, M. & CAL, R. B. 2016 Distribution of mean kinetic energy around an isolated wind turbine and a characteristic wind turbine of a very large wind farm. *Phys. Rev. F* **1** (7), 074402.

DAVENPORT, A. G. 1961 The spectrum of horizontal gustiness near the ground in high winds. *Q. J. R. Meteorol. Soc.* **87** (372), 194–211.

ESPANA, G., AUBRUN, S., LOYER, S. & DEVINANT, P. 2012 Wind tunnel study of the wake meandering downstream of a modelled wind turbine as an effect of large scale turbulent eddies. *J. Wind Engng Ind. Aerodyn.* **101**, 24–33.

JIMENEZ, A., CRESPO, A., MIGOYA, E. & GARCÍA, J. 2008 Large-eddy simulation of spectral coherence in a wind turbine wake. *Environ. Res. Lett.* **3** (1), 015004.

JOHNSON, E., FONTAINE, A. A., JONSON, M. L., MEYER, R. S., STRAKA, W. A., YOUNG, S., VAN DAM, C. P., SHIU, H. & BARONE, M. 2013 A 1:8.7 scale water tunnel test of an axial flow water turbine. In *Proceedings of the 1st Marine Energy Technology Symposium*, METS13, 10–11 April 2013. Washington, DC.

KATZENSTEIN, W., FERTIG, E. & APT, J. 2010 The variability of interconnected wind plants. *Energy Policy* **38** (8), 4400–4410.

KINZEL, M., ARAYA, D. B. & DABIRI, J. O. 2015 Turbulence in vertical axis wind turbine canopies. *Phys. Fluids* **27** (11), 115102.

KOLMOGOROV, A. N. 1941 The local structure of turbulence in incompressible viscous fluid for very large Reynolds numbers. *Dokl. Akad. Nauk SSSR* **30**, 299–303.

KRAICHNAN, R. H. 1964 Kolmogorov's hypotheses and Eulerian turbulence theory. *Phys. Fluids* **7** (11), 1723–1734.

LIGNAROLO, L. E. M., RAGNI, D., SCARANO, F., FERREIRA, C. J. S. & VAN BUSSEL, G. J. W. 2015 Tip-vortex instability and turbulent mixing in wind-turbine wakes. *J. Fluid Mech.* **781**, 467–493.

LIU, H., JIN, Y., TOBIN, N. & CHAMORRO, L. P. 2017 Towards uncovering the structure of power fluctuations of wind farms. *Phys. Rev. E* **96** (6), 063117.

LU, H. & PORTÉ-AGEL, F. 2011 Large-eddy simulation of a very large wind farm in a stable atmospheric boundary layer. *Phys. Fluids* **23** (6), 065101.

LUKASSEN, L. J., STEVENS, R. J. A. M., MENEVEAU, C. & WILCZEK, M. 2018 Modeling space–time correlations of velocity fluctuations in wind farms. *Wind Energy* **21** (7), 474–487.

MILAN, P., WÄCHTER, M. & PEINKE, J. 2013 Turbulent character of wind energy. *Phys. Rev. Lett.* **110** (13), 138701.

PANOFSKY, H. A. & DUTTON, J. A. 1984 *Atmospheric Turbulence: Models and Methods for Engineering Aplications*. Wiley.

SCHLEZ, W. & INFIELD, D. 1998 Horizontal, two point coherence for separations greater than the measurement height. *Boundary-Layer Meteorol.* **87** (3), 459–480.

SHIU, H., VAN DAM, C. P., JOHNSON, E., BARONE, M., PHILLIPS, R., STRAKA, W., FONTAINE, A. & JONSON, M. 2012 A design of a hydrofoil family for current-driven marine-hydrokinetic turbines. In *Proceedings of the 2012 20th International Conference on Nuclear Engineering Collocated with the ASME 2012 Power Conference ICONE20-POWER2012*. American Society of Mechanical Engineers.

SØRENSEN, P., CUTULULIS, N. A., VIGUERAS-RODRÍGUEZ, A., MADSEN, H., PINSON, P., JENSEN, L. E., HJERRILD, J. & DONOVAN, M. 2008 Modelling of power fluctuations from large offshore wind farms. *Wind Energy* **11** (1), 29–43.

STEVENS, R. J. A. M. & MENEVEAU, C. 2014 Temporal structure of aggregate power fluctuations in large-eddy simulations of extended wind-farms. *J. Renew. Energy* **6** (4), 043102.

TABAR, M. R., ANVARI, M., LOHMANN, G., HEINEMANN, D., WÄCHTER, M., MILAN, P., LORENZ, E. & PEINKE, J. 2014 Kolmogorov spectrum of renewable wind and solar power fluctuations. *Eur. Phys. J.-Spec. Top.* **223** (12), 2637–2644.

TENNEKES, H. 1975 Eulerian and Lagrangian time microscales in isotropic turbulence. *J. Fluid Mech.* **67** (3), 561–567.

TIAN, W., OZBAY, A. & HU, H. 2014 Effects of incoming surface wind conditions on the wake characteristics and dynamic wind loads acting on a wind turbine model. *Phys. Fluids* **26** (12), 125108.

TIAN, W., OZBAY, A. & HU, H. 2018 An experimental investigation on the wake interferences among wind turbines sited in aligned and staggered wind farms. *Wind Energy* **21** (2), 100–114.

TOBIN, N., HAMED, A. M. & CHAMORRO, L. P. 2017 Fractional flow speed-up from porous windbreaks for enhanced wind-turbine power. *Boundary-Layer Meteorol.* **163** (2), 253–271.

TOBIN, N., ZHU, H. & CHAMORRO, L. P. 2015 Spectral behaviour of the turbulence-driven power fluctuations of wind turbines. *J. Turbul.* **16** (9), 832–846.

VIGUERAS-RODRÍGUEZ, A., SØRENSEN, P., CUTULULIS, N. A., VIEDMA, A. & DONOVAN, M. H. 2010 Wind model for low frequency power fluctuations in offshore wind farms. *Wind Energy* **13** (5), 471–482.

WILCZEK, M., STEVENS, R. J. A. M. & MENEVEAU, C. 2015 Spatio-temporal spectra in the logarithmic layer of wall turbulence: large-eddy simulations and simple models. *J. Fluid Mech.* **769**, R1.